ISSN 1738-6055 (Print)
ISSN 2233-7660 (Online)

Lab Anim Res 2018: 34(4), 166-175
https://doi.org/10.5625/lar.2018.34.4.166

Laboratory Animal Research
http://submission.kalas.or.kr

CRISPR/Cas9-mediated knockout of *Rag-2* causes systemic lymphopenia with hypoplastic lymphoid organs in FVB mice

Joo-Il Kim[1,2,#], Jin-Sung Park[2,#], Hanna Kim[2], Soo-Kyung Ryu[2], Jina Kwak[2], Euna Kwon[2], Jun-Won Yun[5], Ki-Taek Nam[6], Han-Woong Lee[7], Byeong-Cheol Kang[1,2,3,4,*]

[1]*Graduate School of Translational Medicine, Seoul National University College of Medicine, Seoul, Korea*
[2]*Department of Experimental Animal Research, Biomedical Research Institute, Seoul National University Hospital, Seoul, Korea*
[3]*Biomedical Center for Animal Resource and Development, Seoul National University, College of Medicine, Seoul, Korea*
[4]*Designed Animal and Transplantation Research Institute, Institute of Green Bio Science Technology, Seoul National University, Pyeongchang-gun, Gangwon-do, Korea*
[5]*Department of Biotechnology, The Catholic University of Korea, Bucheon, Gyeonggi-do, Korea*
[6]*College of Medicine Severance Biomedical Science Institute, Yonsei University, Seoul, Korea*
[7]*Department of Biochemistry, Yonsei University, Seoul, Korea*

Recombination activating gene-2 (*RAG-2*) plays a crucial role in the development of lymphocytes by mediating recombination of T cell receptors and immunoglobulins, and loss of *RAG-2* causes severe combined immunodeficiency (SCID) in humans. *Rag-2* knockout mice created using homologous recombination in ES cells have served as a valuable immunodeficient platform, but concerns have persisted on the specificity of *Rag-2*-related phenotypes in these animals due to the limitations associated with the genome engineering method used. To precisely investigate the function of *Rag-2*, we recently established a new *Rag-2* knockout FVB mouse line (*Rag-2*$^{-/-}$) manifesting lymphopenia by employing a CRISPR/Cas9 system at Center for Mouse Models of Human Disease. In this study, we further characterized their phenotypes focusing on histopathological analysis of lymphoid organs. *Rag-2*$^{-/-}$ mice showed no abnormality in development compared to their WT littermates for 26 weeks. At necropsy, gross examination revealed significantly smaller spleens and thymuses in *Rag-2*$^{-/-}$ mice, while histopathological investigation revealed hypoplastic white pulps with intact red pulps in the spleen, severe atrophy of the thymic cortex and disappearance of follicles in lymph nodes. However, no perceivable change was observed in the bone marrow. Moreover, our analyses showed a specific reduction of lymphocytes with a complete loss of mature T cells and B cells in the lymphoid organs, while natural killer cells and splenic megakaryocytes were increased in *Rag-2*$^{-/-}$ mice. These findings indicate that our *Rag-2*$^{-/-}$ mice show systemic lymphopenia with the relevant histopathological changes in the lymphoid organs, suggesting them as an improved *Rag-2*-related immunodeficient model.

Keywords: CRISPR/Cas9, *Rag-2*, histopathology, immunodeficiency, splenic atrophy, thymic atrophy

Received 14 August 2018; Revised version received 4 October 2018; Accepted 5 October 2018

Immune cells play a critical role in protecting vertebrates by detecting and removing foreign substances including pathogens and pathogen-infected cells from the body. Among them, lymphocytes, namely T, B and natural killer (NK) cells, recognize their targets using the immunoglobulin superfamily molecules such as T cell receptors and immunoglobulins through interaction between their antigen binding site and antigens on the targets [1]. To specifically respond to various antigens, the antigen binding site is encoded by a set of small

[#]These authors contributed equally to this work.

*Corresponding author: Byeong-Cheol Kang, Graduate School of Translational Medicine, Seoul National University College of Medicine, 101 Daehakro, Jongno-gu, Seoul 03080, Korea
Tel: +82-2-2072-0841; Fax: +82-2-741-7620; E-mail: bckang@snu.ac.kr

genes composed of a variable (V), a diversity (D), and a joining (J) gene segment, which are selected and rearranged from groups of the individual gene segments through the process called V(D)J recombination [2].

Recombination activating gene-2 (*RAG-2*), encoded by the *RAG-2* gene, is one of the components mediating the V(D)J recombination in the early development stage of T and B cells [2,3]. During the recombination process, *RAG-2* forms a complex with its partner *RAG-1*, stabilizing and extending interaction of *Rag-1* with the recombination signal sequence which exists adjacent to each V, D, and J segment for correct cleavage of the genes [4-7]. Clinically, people carrying mutations in *RAG-2* or *RAG-1,* show Omenn syndrome, an autosomal recessive disease characterized by severe combined immune deficiency (SCID) with autoimmune-like symptoms, demonstrating the essential role of *RAG-2* in immune response [8].

As a model for the disease, *Rag-2* knockout (KO) mouse line was initially generated in 1992 by introducing a PMC1neo cassette in the *Rag-2* exon of embryonic stem (ES) cells using homologous recombination [9]. These mice exhibit SCID phenotypes such as depletion of mature T and B lymphocytes with hypoplastic thymus [9], and therefore have been widely used as an immunodeficient model in diverse fields of research such as etiology of human immune-related disease and xenotransplantation [10].

As exemplified in the *Rag-2* KO models, genome engineering using homologous recombination in ES cells has been extensively utilized in generating mouse disease models. Despite its usefulness, however, the conventional method has disadvantages such as high cost and laborious and time-consuming process for establishment of models [11]. In many cases, insertion of a short DNA fragment like neomycin resistance genes as used in the *Rag-2* KO mice was adopted for disruption of target genes or selection of successfully gene-edited ES clones, which has been reported with adverse impacts on the manifestation of target gene-associated phenotypes [12,13]. Inevitably, these findings have raised concerns on whether the phenotypes of the animals previously generated using such method are specifically related to the targeted genes.

Genome engineering technology has been significantly advanced since the initial introduction of homologous recombination in ES cells. Among the techniques developed to date, CRISPR/Cas9 provides a rapid and site-specific genome editing without using foreign DNA fragments, efficiently overcoming the limitations of the ES cell-based conventional method [14]. For introduction of modification in genome, CRISPR/Cas9 employs a RNA-guided DNA endonuclease enzyme Cas9 and a single strand guide RNA; Cas9 creates a double-strand DNA break at the specific site directed by the guide RNA which is downstream of a protospacer adjacent motif (PAM) sequence (e.g., 5'-NGG-3' for *Streptococcus pyogenes* Cas9) [15-17]. Depending on the presence of repair templates, modification of the targeted genomic site is achieved by non-homologous end joining (NHEJ) or homology-directed repair (HR) when the cellular system repairs the DNA breaks. In addition, CRISPR/Cas9 is generally applied to fertilized eggs with a higher successful rate, significantly reducing the duration to establishment of animal models. With these advantages, CRISPR/Cas9 has rapidly gained popularity among researchers, used in generation of most *in vivo* disease models recently reported in literature [15,18-20].

Previously, we generated a new *Rag-2* KO mouse model using the CRISPR/Cas9 system at Center for Mouse Models of Human Disease (CMHD) (FVB/N-*Rag2*^{em1Hwl}/Korl; *Rag-2*$^{-/-}$ hereafter) and reported immunodeficiency as their major phenotype [21]. In this study, we further characterized their phenotypes by examining histopathological changes in lymphoid organs with monitoring main physiological parameters for 26 weeks, and here report hypoplasitc changes in the lymphoid organs which correlates with severe lymphopenia caused by *Rag-2* deficiency.

Materials and Methods

Animals

Rag-2$^{-/-}$ FVB mice generated using the CRISPR/Cas9 system [21] were used in this study. *Rag-2*$^{-/-}$ mice were born from *Rag-2*$^{+/-}$ parents and used for phenotypic analysis with their wild-type (WT) littermates as a control group. All mice were genotyped 2 weeks after birth using a PCR with specific primers (forward; 5'-CTCCCAGAACTTCAGGATGGGCT-3' and reverse; 5'-AGTCAGGAGTCTCCATCT-CACTGA-3'). Animals of a gender and genotype were housed in a transparent cage under the standard conditions (12 h light/dark cycle, 22±2°C temperature, 40-60% humidity) in a AAALAC International accredited SPF facility (#001169) at Seoul National University Hospital. During the study,

they were given free access to food (LabDiet 5002 Certified Rodent Diet, PMI Nutrition International, USA) and sterilized water. All experiments were approved by the Institutional Animal Care and Use Committee in Seoul National University Hospital and animals were maintained in accordance with Guide for the Care and Use of Laboratory Animals (8th edition, NRC, 2010).

Measurement of main physiological parameters

We started monitoring main physiological parameters of *Rag-2*$^{-/-}$ and WT littermates when they were 4 weeks of age, and terminated at 26 weeks. During this period, animals were daily observed for clinical signs with body weight, food and water consumption measured once a week. Food and water consumption per animal was calculated by using the amount of consumed rodent diet and water per cage during 24 hours. The procedures were carefully carried out during the light cycle with minimal disturbance to animals.

Hematology, serum biochemistry and urinalysis

At the end of 26 weeks, all animals were weighed and sacrificed for hematological and histopathological examination. After induction of deep anesthesia using isoflurane, whole blood was collected from the abdominal vein. 250 μL of blood was collected in K_2EDTA contained tube (BD Microtainer) and analyzed in an ADVIA 2120i (Siemens Healthcare, Tarrytown, NY, USA) for total and differential counting of white blood cells (WBCs) and red blood cells (RBCs), platelets and as well as determination of hemoglobin, mean corpuscular volume, mean corpuscular hemoglobin, and mean corpuscular hemoglobin concentration.

Serum biochemistry was performed using 250 μL of serum in a Hitachi 7070 (Hitachi, Tokyo, Japan) for measurement of blood urea nitrogen, total cholesterol, total protein, aspartate transaminase, alkaline phosphatase, alanine transaminase, albumin, creatinine, triglyceride, glucose, albumin/globulin ratio, potassium, chloride, sodium and phosphorus.

Urine collected from each mice was applied to a urine stick (Multistick 10 SG, Siemens) and analyzed for leukocytes, nitrogen, urobilinogen, protein, pH, blood, specific gravity, ketone, bilirubin and glucose using an automatic urinalysis machine (CLINITEK advantus analyzer, Siemens).

Histopathological analysis

At necropsy, macroscopic examination was carried out on all major organs with recording of any pathological changes. Briefly, each organ was carefully excised after individual weight measurement. Among the organs, testis and epididymis were fixed in Bouin's solution, while Harderian glands and eyes were preserved in Davidson solution. All other organs were fixed in 10% neutral buffered formalin. Fixed organs were embedded in paraffin wax after dehydration in graded ethanol and clearing in xylene, sectioned 4-6 μm thick and stained with hematoxylin and eosin (H&E). Microscopic changes were carefully assessed under a bright-field microscope (BX61, Olympus) with images taken using a DP70 camera (Olympus). Regarding the regions with abnormal changes, images were further analyzed using an Image J software (ver.1.50i, NIH) to quantify the size and number of lesions in the tissue.

Flow cytometry

Spleen, bone marrow and thymus were isolated from age-matched 26 week-old WT and *Rag-2*$^{-/-}$ mice for flow cytometric analysis. The organs were homogenized by passing through 40 μm cell strainer (SPL Life Science). After removing RBC from the isolated cells using a RBC lysis buffer (Invitrogen, USA) and cell counting, 1×10^7 cells were stained with the following antibodies (all antibodies except for anti-NK1.1 (eBioscience, USA) were from BD Bioscience, USA and 1:200 used for all antibodies); V450-anti-CD3ε (500A2) and either FITC-anti-CD4 (RM4-5) or BV605-anti-CD8a (53-6.7) for T cells, V450-anti-IgM (R6-60.2) and PerCP-anti-B220 (RA3-6B2) for B cells, and anti-CD3ε and APC-anti-NK1.1 (PK136;) for NK cells. 20,000 cells were analyzed using a FACSCalibur (BD biosciences). In flow cytometry, cells were selected based on forward and side scatter properties after gating for singlets and each lymphocyte population was gated using fluorescence intensity of the aforementioned antibodies against cell surface markers. Unstained cells were used to set appropriate negative gates by determining the background fluorescence levels, and single stained cells were used as a control to remove spectral overlap between different fluorophores.

Statistical analysis

All values are expressed as mean±standard deviation

(SD). Statistical analysis was performed using two-tailed *t*-test in a SPSS software version 22.0 (SPSS Inc., Chicago, IL, USA). *P* value less than 0.05 was considered as statistically significant.

Results

Rag-2$^{-/-}$ mice developed normally with typical main physiological parameters

Previously, we generated a *Rag-2*$^{-/-}$ FVB mouse line by introducing a deletion of 22 base pairs in exon 3 using a CRISPR/Cas9 system which creates a premature termination codon [21]. These mice showed immunodeficient phenotypes with lack of mature T and B cell population in the spleen and thymus. To further characterize the phenotype of these mice, we analyzed histopathological changes in the lymphoid organs with concurrent examination of circulating WBC with monitoring their development, behavior and main physiological parameters from birth to adulthood. There was no noticeable difference in the number of *Rag-2*$^{-/-}$ male and female mice at birth (male; n=77, female n=82) and the ratio of mice with *Rag-2* KO alleles and WT littermates (*Rag-2*$^{+/+}$:*Rag-2*$^{+/-}$:*Rag-2*$^{-/-}$=1:2.2:0.9), suggesting no effect of *Rag-2* KO on gender determination and the Mendelian inheritance pattern of the mutation. Like their WT littermates, *Rag-2*$^{-/-}$ mice showed normal development and behavior from birth through weaning and puberty to adulthood (data not shown). During 26 weeks, body weight gain (Figure 1), food and water consumption

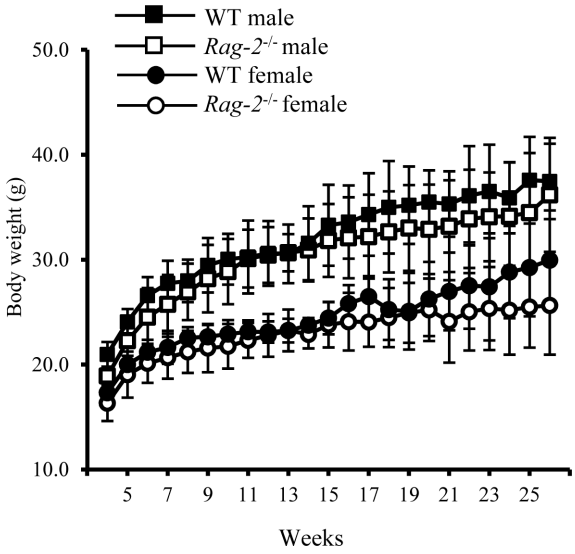

Figure 1. Changes in body weight of wild-type and *Rag-2*$^{-/-}$ mice during 26 weeks. The body weight of wild-type (WT) and *Rag-2*$^{-/-}$ was measured once a week from 4 to 26 weeks of age. During the whole observation period, body weight was similar between WT male (open squares) and *Rag-2*$^{-/-}$ (filled squares), and between WT female (open circles) and *Rag-2*$^{-/-}$ female (filled circles) mice.

(data not shown) of *Rag-2*$^{-/-}$ mice was comparable to their WT littermates. These findings indicate that loss of *Rag-2* have no impact on the physiological development.

Spleen and thymus of *Rag-2*$^{-/-}$ mice were significantly reduced in size and weight

We sacrificed all animals at 26 weeks of age and performed necropsy. Among the major organs examined,

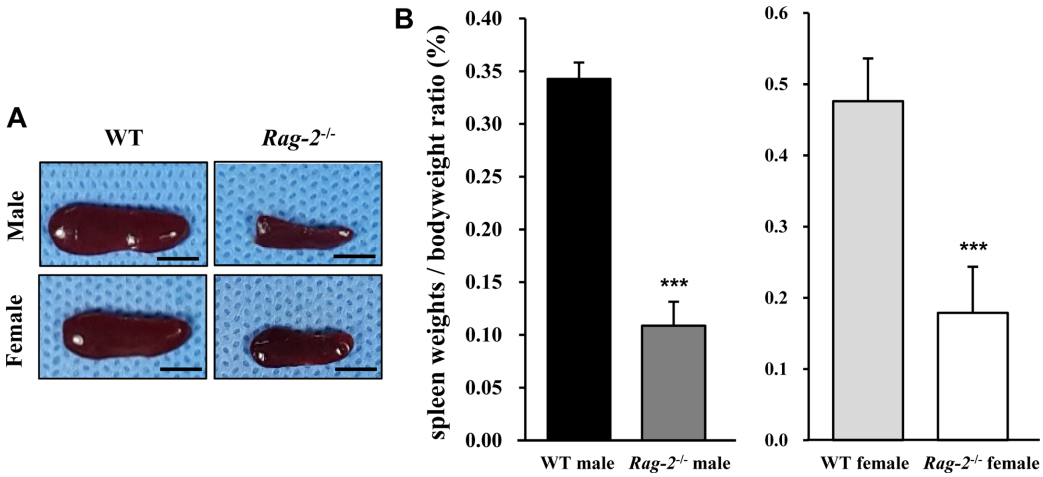

Figure 2. Reduced size and weight of spleen in *Rag-2*$^{-/-}$ mice. (A) Representative photos of spleens from wild-type (WT) and *Rag-2*$^{-/-}$ mice. Scale bar; 5 mm. (B) Relative weight of spleen was significantly reduced in both *Rag-2*$^{-/-}$ male (n=7; dark gray bar) and female (n=8; white bar) mice compared to their respective WT littermates (n=8; black bar for WT male and n=7; light gray bar for WT female). ***P<0.001.

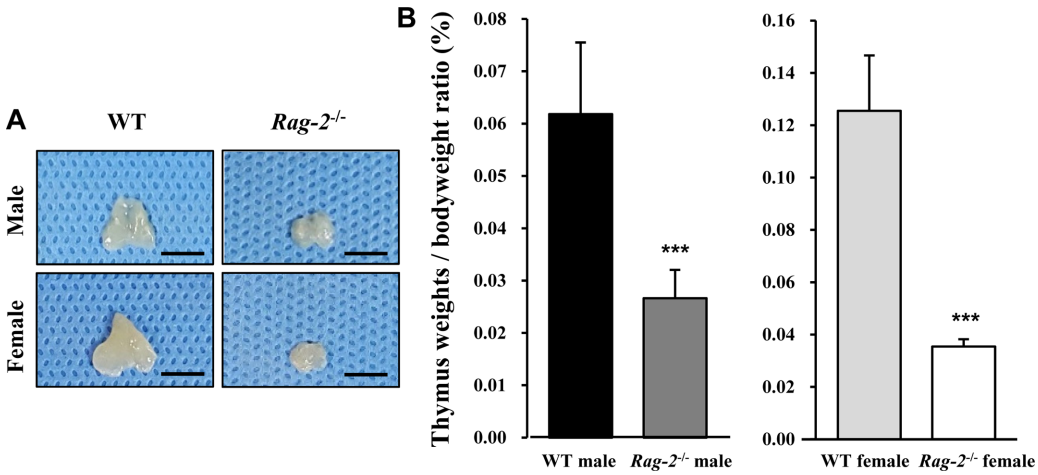

Figure 3. Reduced size and weight of thymus in *Rag-2*$^{-/-}$ mice. (A) Representative photos of thymuses from wild-type (WT) and *Rag-2*$^{-/-}$ mice. Scale bar; 5 mm. (B) Relative weight of thymus was significantly reduced in both *Rag-2*$^{-/-}$ male (n=7; dark gray bar) and female (n=8; white bar) mice compared to their respective WT littermates (n=8; black bar for WT male and n=7; light gray bar for WT female). ***P<0.001.

both spleens (Figure 2A) and thymuses (Figure 3A) of *Rag-2*$^{-/-}$ mice were remarkably smaller than those of WT mice. When calculated, relative organ weight was found to be significantly decreased for the spleens (Figure 2B and Table 1; P<0.001) and thymuses (Figure 3B and Table 1; P<0.001) in both *Rag-2*$^{-/-}$ male and female mice compared to their respective gender-matching WT littermates. Notably, no *Rag-2*-related changes in actual and relative weight were observed in all the other organs of *Rag-2*$^{-/-}$ mice (Table 1).

Table 1. Absolute and relative weight of major organs of *Rag-2*$^{-/-}$ mice

Organ		WT male	*Rag-2*$^{-/-}$ male	WT female	*Rag-2*$^{-/-}$ female
		(n=8)	(n=7)	(n=7)	(n=8)
Body weight	(g)	36.2±5.4	37.5±3.6	25.6±4.7	30.0±4.7
Liver	(g)	1.559±0.334	1.608±0.118	1.242±0.165	1.400±0.216
	(g%)	4.296±0.559	4.313±0.396	4.877±0.257	4.714±0.646
Spleen	(g)	0.120±0.019	0.041±0.010***	0.113±0.010	0.052±0.016***
	(g%)	0.332±0.030	0.108±0.023***	0.449±0.065	0.177±0.064***
Kidney (right)	(g)	0.222±0.099	0.241±0.033	0.153±0.019	0.167±0.019
	(g%)	0.616±0.251	0.647±0.095	0.605±0.085	0.565±0.087
Kidney (left)	(g)	0.237±0.036	0.223±0.037	0.145±0.021	0.152±0.016
	(g%)	0.656±0.057	0.595±0.082	0.574±0.094	0.591±0.100
Adrenal gland	(g)	0.001±0.000	0.001±0.000	0.005±0.000	0.006±0.001*
(right)	(g%)	0.003±0.001	0.003±0.001	0.020±0.003	0.019±0.003
Adrenal gland	(g)	0.001±0.000	0.001±0.000	0.006±0.001	0.007±0.001
(left)	(g%)	0.003±0.001	0.003±0.001	0.024±0.002	0.022±0.003
Testis (right)	(g)	0.110±0.029	0.100±0.007	0.005±0.002	0.004±0.001
/ovary (right)	(g%)	0.307±0.077	0.268±0.028	0.020±0.007	0.016±0.006
Testis (left)	(g)	0.100±0.006	0.096±0.006	0.005±0.001	0.004±0.001
/ovary (left)	(g%)	0.280±0.033	0.257±0.023	0.019±0.007	0.014±0.006
Thymus	(g)	0.021±0.003	0.011±0.002***	0.030±0.006	0.010±0.001***
	(g%)	0.059±0.011	0.028±0.005***	0.117±0.011	0.035±0.002***
Heart	(g)	0.160±0.018	0.172±0.020	0.137±0.016	0.140±0.026
	(g%)	0.444±0.021	0.458±0.036	0.545±0.100	0.477±0.118
Lung	(g)	0.159±0.020	0.165±0.012	0.149±0.015	0.145±0.007
	(g%)	0.443±0.046	0.442±0.038	0.593±0.080	0.495±0.072*
Brain	(g)	0.501±0.031	0.526±0.038	0.498±0.027	0.515±0.032
	(g%)	1.404±0.168	1.412±0.127	1.978±0.234	1.746±0.222

*P<0.05 and ***P<0.001 in comparison to respective gender-matching WT mice

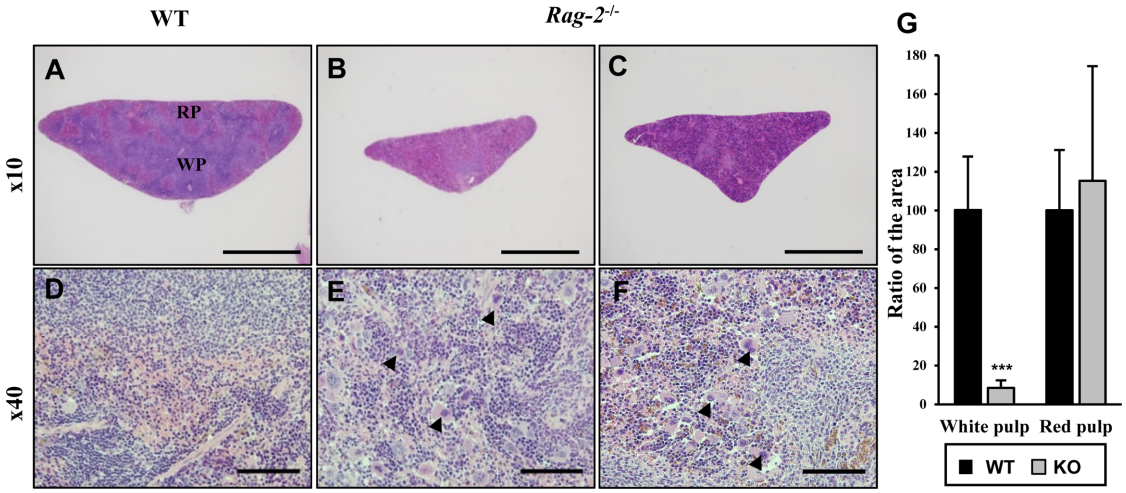

Figure 4. Shrinkage of splenic white pulps with intact red pulps in *Rag-2*$^{-/-}$ mice. H&E stained sections of spleens were examined for microscopic changes. (A-C) Cross sections of wild-type (WT) spleen (A) shows the white pulp (WP) and red pulps (RP), while WPs in the spleen of *Rag-2*$^{-/-}$ became less abundant and smaller (B and C). Scale bars; 500 μm. (D-F) Compared to a dense population of lymphocytes in WT WP (D), *Rag-2*$^{-/-}$ mice (E and F) show an evident decrease with an increased number of megakaryocytes (arrowheads). Scale bars; 5 μm. (G) Quantification of area confirmed the reduction of WPs in *Rag-2*$^{-/-}$ mice (dark gray bars) in comparison with WT (black bars), while RPs remained unchanged. ***P<0.001.

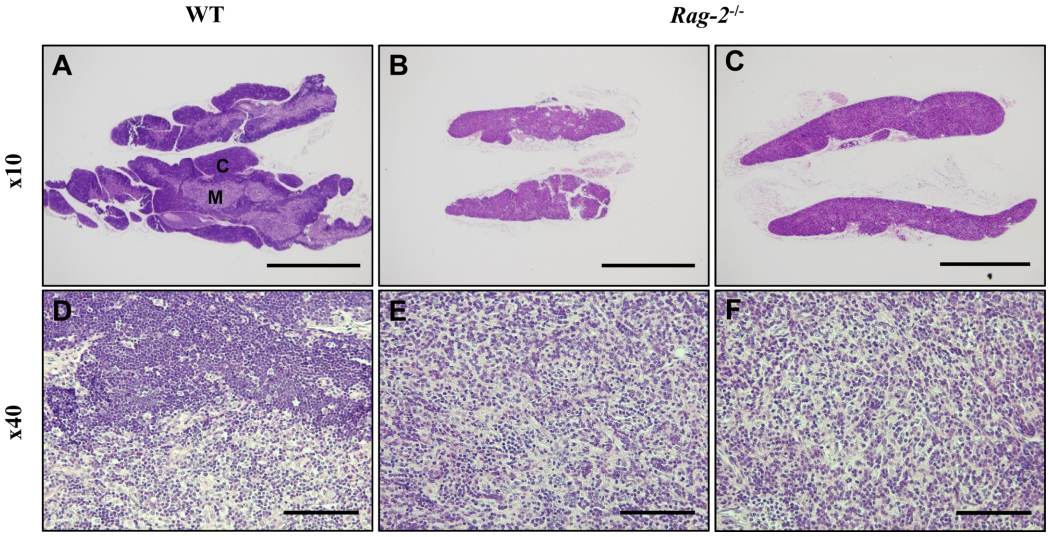

Figure 5. Atrophy of thymic cortex in *Rag-2*$^{-/-}$ mice. H&E stained sections of thymuses were examined for microscopic changes. (A) Low-powered image of WT thymus depicts a well-demarcated layer of the cortex (C) with the medulla (M) forming the inner part, while (B and C) *Rag-2*$^{-/-}$ thymus shows disappearance of the cortex. Scale bars; 500 μm. As opposed to the existence of lymphocyte-populated cortex in WT (D), higher magnification confirmed the loss of thymic cortex in *Rag-2*$^{-/-}$ (E and F). Scale bar; 5 μm.

Histopathological analysis of the lymphoid organs in *Rag-2*$^{-/-}$ mice

Lymphoid organs including spleen, thymus, lymph nodes and bone marrow were fixed and processed for microscopic examination. H&E staining revealed that when compared to WT littermates (Figure 4A), the white pulp in the spleens of *Rag-2*$^{-/-}$ mice was significantly diminished (Figure 4B, 4C), while the red pulp was seemingly unchanged. At cellular levels, a remarkable decrease of lymphocytes from the spleens of *Rag-2*$^{-/-}$ mice was noticed (Figure 4D-4F). Quantification of the area occupied by the white and red pulp confirmed our visual findings; with the values for WT set at 100%, the area of *Rag-2*$^{-/-}$ splenic white pulp was only 8.5% (P<0.001), while that of the red pulp was 115.3% (Figure 4G). Interestingly, megakaryocytes were more frequently observed in the spleens of *Rag-2*$^{-/-}$ mice.

In thymuses, low-powered photomicrographs showed that in comparison with the normal structure of the cortex and medulla in WT (Figure 5A), the cortex in

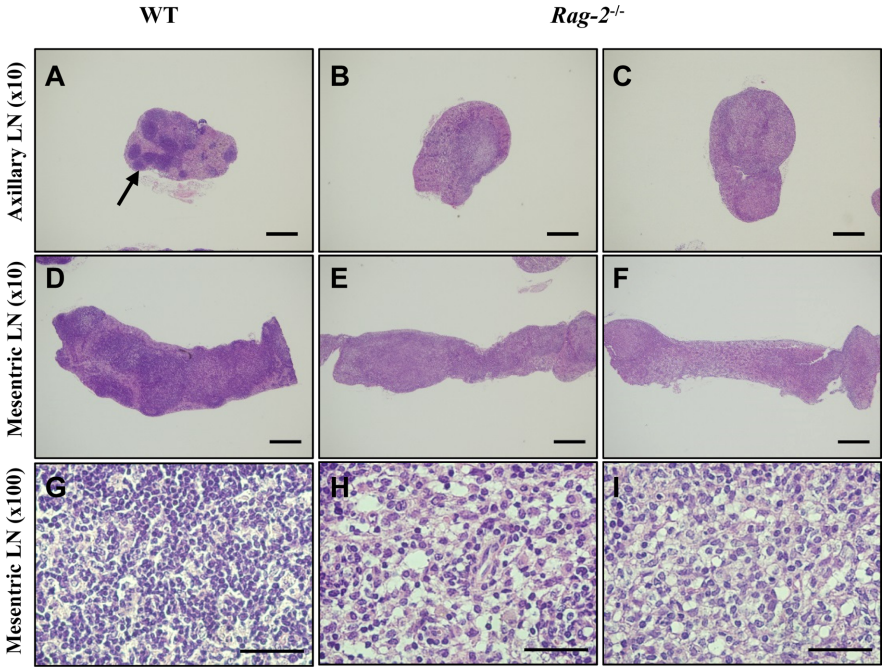

Figure 6. Reduction of primary and secondary follicles in *Rag-2*$^{-/-}$ lymph nodes. Axillary and mesenteric lymph nodes embedded in paraffin were sectioned and stained with H&E. Axillary (A) and mesenteric (D) lymph nodes of wild-type (WT) mice show well-developed primary and secondary follicles with a high number of lymphocytes in these structure (G). On the contrary, neither such follicles (B and C for the axillary and E and F for the mesenteric lymph nodes) nor groups of lymphocytes (E and F) are observed in *Rag-2*$^{-/-}$ lymph nodes. Scale bars in (A-D) and (E and F) are 200 and 5 μm, respectively.

Rag-2$^{-/-}$ mice completely disappeared, leaving the medulla only in the thymus (Figure 5B, 5C). Higher magnification uncovered that loss of lymphocytes is the cause of such difference in the thymus between WT (Figure 5D) and *Rag-2*$^{-/-}$ (Figure 5E, 5F). Similarly, the lymphoid follicles in the axillary (Figure 6A-6C) and mesenteric lymph nodes (Figure 6D-6F) were hardly observed in *Rag-2*$^{-/-}$ mice due to significant reduction of lymphocytes as shown in the mesenteric lymph nodes (Figure 6G-6I). Unlike these changes, bone marrow of *Rag-2*$^{-/-}$ mice appeared normal without noticeable changes in gross and microscopic examinations (data not shown).

The composition of WBC in peripheral blood was altered in *Rag-2*$^{-/-}$ mice

Reduction of lymphocytes in the lymphoid organs may decrease circulating lymphocytes in the blood and impact on the populations of other leukocytes. To determine the effect of *Rag-2* KO on blood WBC profiles, we performed differential counting of WBC acquired from the peripheral blood. Total number of WBC was significantly decreased in both *Rag-2*$^{-/-}$ male and female mice compared with WT (Figure 7A; $P<0.001$ for both). A detailed profiling of each type of WBC revealed that lymphocytes were significantly decreased in both genders of *Rag-2*$^{-/-}$ mice (Figure 7B; $P<0.001$ for both), while no other types of WBC showed a meaningful change except for mild but significant reduction observed in the count of neutrophils and basophils in *Rag-2*$^{-/-}$ male mice, indicating that the specific reduction of lymphocytes is responsible for leukocytopenia in the blood. Contrary to these findings, platelet counts were markedly increased (Figure 7E; $P<0.001$). No changes were observed in the number of reticulocytes (Figure 7F), indicating normal erythropoiesis. In addition, all parameters measured in serum chemistry and urinalysis were comparable between WT and *Rag-2*$^{-/-}$ mice (data not shown).

Loss of mature T and B cells with increased NK cells in lymphoid organs of *Rag-2*$^{-/-}$ mice

Our findings in histopathological and hematological analyses suggested profound reduction of lymphocytes due to the loss of *Rag-2*. To investigate the changes of individual lymphocyte populations in details, we performed flow cytometry on the cells isolated from the lymphoid organs (Figure 8). Our analysis revealed a

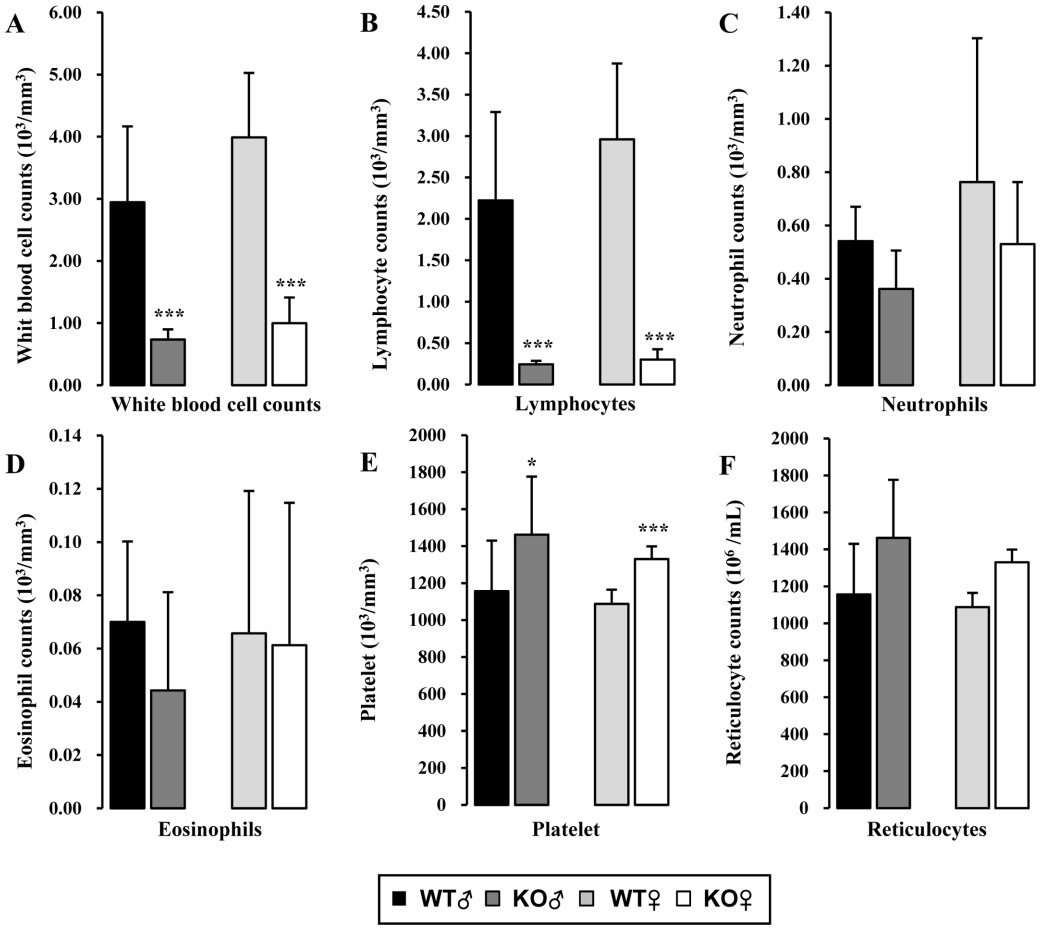

Figure 7. Hematologic analysis of peripheral blood of *Rag-2*$^{-/-}$ mice. (A) Total white blood cell count was significantly decreased in both *Rag-2*$^{-/-}$ male (dark gray bars) and female (white bars) mice compared with their gender-matching wild-type (WT) littermates (black bars for WT male and light gray bars for WT female). The number of lymphocytes (B) was similarly decreased in both gender of *Rag-2*$^{-/-}$ mice, while neutrophils (C) and eosinophils (D) remained unchanged. (E) On the contrary, platelets were more abundant in *Rag-2*$^{-/-}$ mice. (F) There was no change in the number of reticulocytes. **P*<0.05 and ****P*<0.001

complete loss of both $CD3e^+CD4^+$ helper and $CD3e^+$ $CD8^+$ cytotoxic T cells from the spleens (Figure 8A, 8B) and thymuses (Figure 8E, 8F) of *Rag-2*$^{-/-}$ mice. Furthermore, $B220^+IgM^+$ B cells were also markedly decreased in the spleens and bone marrow (Figure 8D, 8H). Interestingly, NK cells which express NK1.1 but not CD3e increased in *Rag-2*$^{-/-}$ mice by 5 folds in the spleen (Figure 8C) and 11 folds in the thymus (Figure 8G) compared to WT.

Discussion

CRISPR/Cas9 has become a popular genome editing technology for generating disease model animals by overcoming several limits of the conventional methods. Using this system, we recently established a new *Rag-2*$^{-/-}$ mouse line which manifested immunodeficiency as the major phenotype. In this study, we histopathologically characterized the immunophenotype of 26-week-old *Rag-2*$^{-/-}$ mice. Our data show structural alteration in the spleen, thymus and lymph nodes with the concurrent changes in the peripheral blood of *Rag-2*$^{-/-}$ mice due to systematic loss of mature T and B cells.

Knockout of *Rag-2* using the CRISPR/Cas9 system did not seem to affect the normal development and aging of FVB mice; Beyond the 8 weeks of normal development we previously reported [21], our *Rag-2*$^{-/-}$ mice did not show any noticeable difference from WT littermates in all the parameters measured here up to 26 weeks.

Among the organs examined at necropsy, spleen and thymus were found to be the most affected, consistent with our previous findings [21]; gross examination revealed that their size and weight in *Rag-2*$^{-/-}$ mice were markedly reduced in comparison to WT littermates.

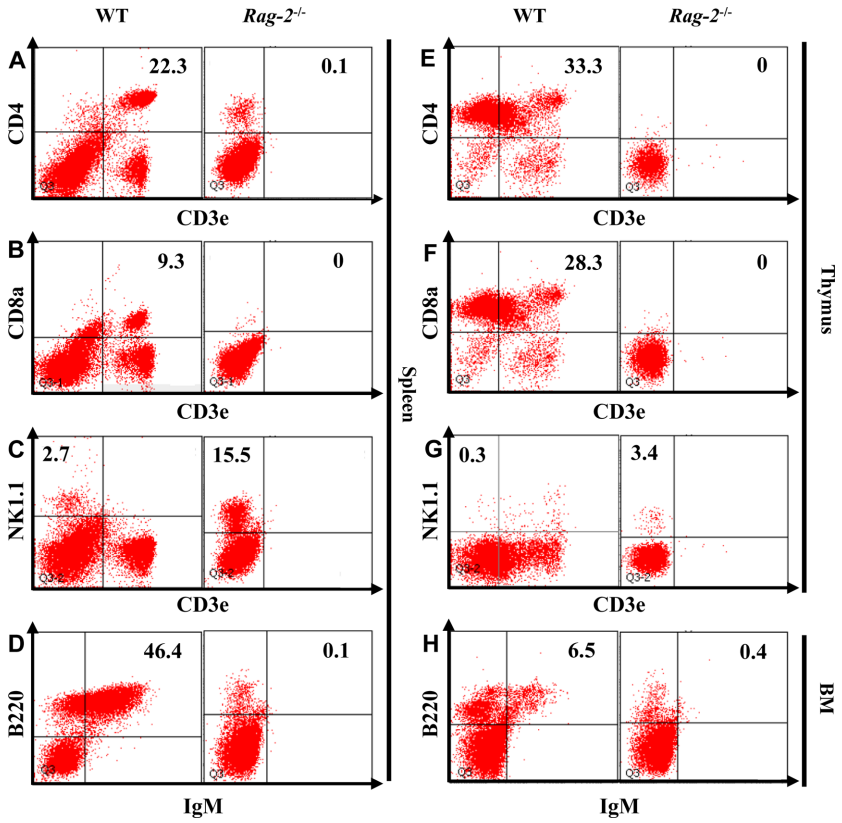

Figure 8. Flow cytometric analysis of lymphocytes isolated from the lymphoid organs of *Rag-2*$^{-/-}$ mice. The cells were isolated from spleen, thymus and bone marrow (BM) after homogenization and stained with appropriate antibodies to mark B, T and natural killer (NK) cells. CD3e^{+}CD4^{+} and CD3e^{+}CD8a^{+} T cells were depleted from spleen (A and B) and thymus (E and F) of *Rag-2*$^{-/-}$ mice, while the number of CD3e^{-}NK1.1^{+} NK cells (C and G) was markedly increased in these lymphoid organs. Spleen and BM also showed a significant reduction of IgM^{+}/B220^{+} B cells.

Unlike the original *Rag-2* KO mice generated by the conventional ES cell-based system which showed similarly smaller thymuses with a normal range of spleens [9], our *Rag-2*$^{-/-}$ mice had decreased sizes of both organs, demonstrating them as a histopathologcially improved model system.

Previously, loss of *Rag-2* was shown to block T and B cell differentiation by impairing the V(D)J recombination, depleting mature lymphocytes [9]. In line with these findings, we found a significant reduction of lymphocytes on histopathologcial examination of the lymphoid organs, which revealed severe atrophy of the splenic white pulp as well as the thymic cortex. Furthermore, axillary and mesenteric lymph nodes also showed rudimentary primary and secondary follicles, confirming the structural alteration due to lymphopenia. Consistently, our data from flow cytometry showed a complete loss of CD3e^{+}CD4^{+} helper and CD3e^{+}CD8^{+} cytotoxic T cells from the spleen and thymus as well as mature B cells from the spleen and bone marrow. In addition, ablation of *Rag-2* also effectively reduced peripheral lymphocytes from the blood, leaving neutrophils as the major type of WBC. Notably, there was no noticeable change in the number of granulocytes in the peripheral blood except for incidental decrease of neutrophils and basophils observed in *Rag-2*$^{-/-}$ male mice, negating compensatory proliferation of other WBC populations. These results, together with the previous reports on the original *Rag-2* KO mice as well as our previous findings [21], confirmed the SCID phenotype of our *Rag-2*$^{-/-}$ mice.

Despite the loss of mature T and B cells from the spleens and thymuses of *Rag-2*$^{-/-}$ mice, NK cells in these organs were upregulated as demonstrated in Figure 8, consistent with the previous reports [21]. Furthermore, we also found that megakaryocytes were increased in the spleens of *Rag-2*$^{-/-}$ mice as shown in Figure 4, but not in the bone marrow (data not shown), collectively suggesting activation of a compensatory mechanism for lack of functional T and B cells. The higher levels of lymphocytes and platelets than the normal ranges in *Rag-2*$^{-/-}$ mice

were likely caused by an increased influx from the lymphoid organs into the blood stream as part of the compensatory changes. Although it is likely NK cells that contributed to maintaining the levels of lymphocytes in the blood of *Rag-2*$^{-/-}$ mice, whether NK cells are the sole cause or other cells such as immature lymphocytes also concomitantly responsible still remains unclear. Also, understanding the roles of these NK cells and platelets in the immune response of *Rag-2*$^{-/-}$ mice is of great interest. Further investigation may be required to elucidate the composition of residual lymphocytes in peripheral blood as well as the function of the elevated levels of NK cells and platelets in *Rag-2*$^{-/-}$ mice.

In this study, we investigated histopathological changes in the lymphoid organs of a new *Rag-2*$^{-/-}$ FVB mouse line which was generated using the CRISPR/Cas9 system. Our results in the study indicate that our mice have a SCID phenotype with severe lymphopenia accompanying microstructural changes in the relevant lymphoid organs due to systemic depletion of mature T and B cells, while developing normally up to 26 weeks without *Rag-2* related issues. Although similar phenotypes have been reported in the original *Rag-2* KO mice, our mice are a better model for *Rag-2* deficiency due to the following reasons; unlike the original KO, our mice 1) do not carry a Neo cassette and therefore facilitate manifestation of the phenotype purely related to loss of *Rag-2*, and 2) have histopathological alternations in both thymus and spleen which are consistent with the loss of mature T cells in these organs as well as peripheral blood. Taken together, our findings demonstrate the usefulness of our *Rag-2*$^{-/-}$ mice, providing them as an improved model for *RAG-2*-related human diseases and research into its function.

Acknowledgments

This research was supported by a grant (14182 MFDS978) from Ministry of Food and Drug Safety in 2015.

Conflict of interests The authors declare that there is no financial conflict of interests to publish these results.

References

1. Nalefski EA, Kasibhatla S, Rao A. Functional analysis of the antigen binding site on the T cell receptor alpha chain. J Exp Med 1992; 175(6): 1553-1563.
2. Tonegawa S. Somatic generation of antibody diversity. Nature 1983; 302(5909): 575-581.
3. Gellert M. V(D)J recombination: RAG proteins, repair factors, and regulation. Annu Rev Biochem 2002; 71(1): 101-132.
4. McBlane JF, van Gent DC, Ramsden DA, Romeo C, Cuomo CA, Gellert M, Oettinger MA. Cleavage at a V(D)J recombination signal requires only RAG1 and RAG2 proteins and occurs in two steps. Cell 1995; 83(3): 387-395.
5. Oettinger MA, Schatz DG, Gorka C, Baltimore D. *RAG-1* and *RAG-2*, adjacent genes that synergistically activate V(D)J recombination. Science 1990; 248(4962): 1517-1523.
6. Schatz DG, Oettinger MA, Baltimore D. The V(D)J recombination activating gene, *RAG-1*. Cell 1989; 59(6): 1035-1048.
7. Xu K, Liu H, Shi Z, Song G, Zhu X, Jiang Y, Zhou Z, Liu X. Disruption of the RAG2 zinc finger motif impairs protein stability and causes immunodeficiency. Eur J Immunol 2016; 46(4): 1011-1019.
8. Villa A, Santagata S, Bozzi F, Imberti L, Notarangelo LD. Omenn syndrome: a disorder of Rag1 and Rag2 genes. J Clin Immunol 1999; 19(2): 87-97.
9. Shinkai Y, Rathbun G, Lam KP, Oltz EM, Stewart V, Mendelsohn M, Charron J, Datta M, Young F, Stall AM, *et al*. *RAG-2*-deficient mice lack mature lymphocytes owing to inability to initiate V(D)J rearrangement. Cell 1992; 68(5): 855-867.
10. Ito M, Hiramatsu H, Kobayashi K, Suzue K, Kawahata M, Hioki K, Ueyama Y, Koyanagi Y, Sugamura K, Tsuji K, Heike T, Nakahata T. NOD/SCID/gamma(c)(null) mouse: an excellent recipient mouse model for engraftment of human cells. Blood 2002; 100(9): 3175-3182.
11. Skarnes WC. Is mouse embryonic stem cell technology obsolete? Genome Biol 2015; 16(1): 109.
12. Valera A, Perales JC, Hatzoglou M, Bosch F. Expression of the neomycin-resistance (neo) gene induces alterations in gene expression and metabolism. Hum Gene Ther 1994; 5(4): 449-456.
13. Scacheri PC, Crabtree JS, Novotny EA, Garrett-Beal L, Chen A, Edgemon KA, Marx SJ, Spiegel AM, Chandrasekharappa SC, Collins FS. Bidirectional transcriptional activity of PGK-neomycin and unexpected embryonic lethality in heterozygote chimeric knockout mice. Genesis 2001; 30(4): 259-263.
14. Wang H, Yang H, Shivalila CS, Dawlaty MM, Cheng AW, Zhang F, Jaenisch R. One-step generation of mice carrying mutations in multiple genes by CRISPR/Cas-mediated genome engineering. Cell 2013; 153(4): 910-918.
15. Cong L, Ran FA, Cox D, Lin S, Barretto R, Habib N, Hsu PD, Wu X, Jiang W, Marraffini LA, Zhang F. Multiplex genome engineering using CRISPR/Cas systems. Science 2013: 339(6121): 819-823.
16. Jiang W, Bikard D, Cox D, Zhang F, Marraffini LA. RNA-guided editing of bacterial genomes using CRISPR-Cas systems. Nat Biotechnol 2013; 31(3): 233-239.
17. Jinek M, Chylinski K, Fonfara I, Hauer M, Doudna JA, Charpentier E. A programmable dual-RNA-guided DNA endonuclease in adaptive bacterial immunity. Science 2012; 337(6096): 816-821.
18. Ran FA, Hsu PD, Lin CY, Gootenberg JS, Konermann S, Trevino AE, Scott DA, Inoue A, Matoba S, Zhang Y, Zhang F. Double nicking by RNA-guided CRISPR Cas9 for enhanced genome editing specificity. Cell 2013; 154(6): 1380-1389.
19. Doudna JA, Charpentier E. Genome editing. The new frontier of genome engineering with CRISPR-Cas9. Science 2014; 346(6213): 1258096.
20. Hsu PD, Lander ES, Zhang F. Development and applications of CRISPR-Cas9 for genome engineering. Cell 2014; 157(6): 1262-1278.
21. Lee JH, Park JH, Nam TW, Seo SM, Kim JY, Lee HK, Han JH, Park SY, Choi YK, Lee HW. Differences between immunodeficient mice generated by classical gene targeting and CRISPR/Cas9-mediated gene knockout. Transgenic Res 2018: 241-251.